www.sciencemag.org/cgi/content/full/science.1232389/DC1

Supplementary Materials for

Wnt Stabilization of β-Catenin Reveals Principles for Morphogen Receptor-Scaffold Assemblies

Sung-Eun Kim, He Huang, Ming Zhao, Xinjun Zhang, Aili Zhang, Mikhail V. Semonov, Bryan T. MacDonald, Xiaowu Zhang, Jose Garcia Abreu, Leilei Peng, Xi He*

*Corresponding author. E-mail: xi.he@childrens.harvard.edu

Published 11 April 2013 on *Science* Express
DOI: 10.1126/science.1232389

This PDF file includes:

Materials and Methods
Figs. S1 to S18
References

Materials and Methods

Plasmid constructs

Mouse Axin (Flag-tagged), Wnt3a, LDLRΔN, LRP6ΔN, GST-β-catenin and GST–LRP6C have been described (*3*, *5*, *6*). DNA sequences for Myc-tagged Axin-DIX, Axin-BCD (β-catenin binding domain), and Dvl-DIX were subcloned into pGEX4T-2 vectors, and for GFP-Axin-mCherry were subcloned into pcDNA3.1. Various mutations were introduced in the above Axin, Axin-BCD, Axin-DIX, and GFP-Axin-mCherry by Quickchange Kit (Stratagene) according to the manufacturer's instruction, and were confirmed by sequencing. cDNAs for Human and Xenopus I2 (PPP1R2) were obtained via RT-PCR from RNAs of HEK293T cells and stage 26 Xenopus laevis embryos, respectively, and were cloned into pEF1α, pCS2+myc and pCS2+Flag vectors. Detailed information for constructs is available upon request.

Antibodies

Ab-pS497/500, the anti-phospho-Axin (Ser497/500) antibody, was generated in rabbits (Covance) using synthetic phospho-peptide (CPGHRpSPDpSGHVAK) as the immunogen. Sera were purified using affinity columns (Pierce) of the phospho-peptide and the corresponding regular peptide (with the two serines unphosphorylated), respectively, and subsequently dialyzed against PBS buffer. The specificity of the antibody was verified first via dot-blotting (data not shown) and then via immunoblotting assays (fig. S1).

All other commercial antibodies were used in accordance with the manufacturers' instructions: anti-LRP6, anti-phopho-LRP6 (Ser 1490), anti-Axin, anti-phospho-β-catenin (S33/S37/T41), anti-GSK3β (Cell Signaling); anti-Flag, M2 (Sigma); anti-β-actin, anti-β-tubulin, anti-Myc (9E10) (Santa Cruz); anti-β-catenin, anti-I2 (BD Transduction Lab); and anti-GSK3α/β and anti-PP1 (Millipore).

Immunoblotting, Immunoprecipitation, and immunofluorescence

Cell lysates were prepared 40-48 hours after transfection in a RIPA buffer or buffer containing 50 mM HEPES (pH 7.4), 1.5 mM EDTA, 150 mM NaCl, 10% glycerol, 1% triton X-100, 0.5 mM DTT and a cocktail of phosphatase and protease inhibitors (Roche). Immunoblotting was performed as described (*6*). For preparation of HEK293T cytosolic extracts for β-catenin detection, cells were lysed with 0.015% digitonin in PBS containing a cocktail of protease inhibitors and phosphatase inhibitors (Roche). For immunoprecipitations, cell lysates from HEK293T or L cells were incubated with the primary antibody for 2-4 hours at 4°C, followed by addition of 50% slurry of protein G-sepharose and overnight incubation at 4°C. Precipitates were washed with lysis buffer and boiled with 2xSDS sample buffer before loading for SDS-PAGE. For Immunoflouresence, HeLa cells were grown on the coverslips and transfected with GFP-Axin-mCherry (Axin: WT or M2M4), and fixed with 3.7% paraformaldehyde for 30 minutes at RT. The coverslips were washed, mounted on glass slides and imaged by confocal microscopy (Carl-Zeiss LSM510).

Cell culture, transfection, infection, stable cell lines and luciferase assays

HEK293T, RKO, L, and HeLa cells were cultured in DMEM medium supplemented with 10% Fetal Bovine Serum (FBS). WT and Gsk3α;Gsk3β-/- mouse ES cells were cultured as described previously (*26*). Tautomycin (TM), BIO, and SB216763 (Calbiochem) were purchased and used according to the manufacturer's instruction (TM: 2 μM; Bio: 2 μM; SB216763: 20 μM). Cells were treated with recombinant human WNT3A (StemR&D) at 100 ng/ml and the pharmacological inhibitors for 2 hours unless specified otherwise. Cells were transfected using Fugene 6, Fugene HD transfection reagent (Promega) or Lipofectamine 2000 (Invitrogen) according to the manufacturer's instruction. shRNA constructs against human I2 (accession NM_006241) were purchased from Sigma Mission shRNA library. For shRNA viral infections, HEK293T or RKO cells were transfected with an shRNA construct and viral packaging constructs (tat, VSVG, Gag) and viral medium was collected 48 hours or 60 hours after transfection. The medium was filtered with 0.45μm filter and cells were infected for 6-18 hours. A viral vector for GFP expression was used as an infection efficiency control. For stable cDNA-expressing cells used in live or fixed cell imaging, HeLa cells were transfected with an expression vector for GFP-Axin-mCherry or GFP-AxinM2M4-mCherry or other derivatives and were selected by neomycin. Luciferase reporter assays were performed in triplicate by plating HEK293T cells in 24-well plates as described (*5*, *6*), using Dual Luciferase Reporter Assay System (Promega) according to the manufacturer's instruction.

cDNA library screening

FLEXGene BC1000 (Harvard Proteomics Institute), a collection of 1000 human cDNAs that are associated with breast cancer via various criteria, was used for functional expression screening in a pJP1520 retroviral expression vector. HEK293T cells were transiently transfected with a single cDNA and the TOP-Flash reporter.

In vitro binding and phosphorylation assays

For GST pull-down assays, each bacterially expressed GST fusion protein was purified and immobilized on glutathione sepharose beads (Amersham Bioscience) and mixed with cell lysates for 2 hours at 4°C. Samples were subsequently washed at least three times and boiled with 2xSDS sample buffer before loading for SDS-PAGE and immunoblotting. GST-LRP6C on Glutathione Sepharose beads was incubated without or with GSK3 and CK1 (NEB) for 4 hours at 30°C and then washed repeatedly to remove the kinases. GST-phospho-LRP6C was then incubated for 2 hours at 4°C with HEK293T lysates, as was GST-β-catenin. GST-Axin-BCD was immobilized on Glutathione Sepharose beads and incubated with or without GSK3 for 4 hours at 30°C. GST-Axin-DIX and mutants (Myc-tagged), GST-Dvl-DIX (Myc-tagged), and GST-β-catenin were purified and cleaved by incubation with thrombin (Sigma) for 2 hours at RT. These purified and cleaved recombinant Axin-DIX and mutants (Myc-tagged), Dvl-DIX (Myc-tagged), and β-catenin were then used for in vitro GST-Axin-BCD pull-down assays.

Xenopus embryo manipulation, injection, and in situ hybridization

Procedures for animal staging, injection and hybridization have been described (*31*). Synthetic RNAs were transcribed in vitro with MessageMachine (Ambion). The Xenopus

I2 Morpholino oligonucleotide (5'-GCCGCCATGTTCCCAGAGTTACACA-3') and β-catenin Morpholino oligonucleotide (5'- TTTCAACCGTTTCCAAAGAACCAGG -3') (*32*) were synthesized by GeneTools and was injected at 10 or 20 ng/embryo. For embryos receiving injection of the I2MO plus the β-catenin MO, the I2MO or a control MO (20ng/embryo) was injected first into animal dorsal blastomeres at the 8-cell stage, and the β-catenin MO or the control MO (20ng/embryo) was injected into the 4-dorsal animal cells (A-tier) at the 32-cell stage as previously described (*32*). The control MO was used to balance the amount of injected MOs.

FLIM and Fluorescence Anisotropy Imaging

For live cell imaging, we used either HeLa cells stably expressing with GFP-AxinM2M4-mCherry or HeLa cells transiently expressing GFP-AxinM2M4-mCherryYA. Fluorescence lifetime imaging microscopy (FLIM) of live HeLa cells was performed on a confocal microscope based on Fourier lifetime spectroscopy (*33*). This FLIM confocal microscope acquires fluorescence lifetime images of GFP and mCherry simultaneously to avoid possible artifacts from photobleaching of the fluorescent proteins. Excitation lasers for GFP (488 nm) and mCherry (561 nm) were combined and modulated at different frequencies by a Michelson interferometer. The modulated excitation was used as the light source of a confocal scanning microscope to excite both GFP and mCherry. Fluorescence emissions associated with GFP (525±20 nm) and mCherry (593±20 nm) were detected by two separate PMT (Hamamatsu H7420) simultaneously and correlated with laser modulations to perform frequency domain fluorescence lifetime imaging. The two-color lifetime image was acquired at 10 second per 400-by-400 frame with a 60X NA1.4 oil objective lens. Lifetime of GFP and mCherry was fitted with the single exponential decay model with programs written in Matlab, using fluorescein (488 nm excitation) and Rhodamine B (561nm excitation) as lifetime references.

For fixed cell imaing, HeLa cells were plated on cover glasses in the 24-well plates, and were transiently transfected with GFP-AxinM2M4-mCherry. After washing with PBS, cells were fixed with 4% formaldehyde, and mounted onto glass slides, and GFP lifetime images were acquired as above.

Fluorescence anisotropy images of HeLa cells were acquired with the same confocal microscope, with the exception that the fluorescence emission was separated by a polarized beam splitter into parallel and perpendicular polarization signals relative the polarization of the laser. Two polarized signals were detected by two PMT simultaneously. Two-channel polarization sensitive images were acquired at 10 second per frame. To avoid the depolarization effect of a high NA objective lens, a 40X 0.75 NA dry lens was use to collect images. Fluorescence anisotropy images were calculated from polarization image pairs.

Each pixel histogram was summarized from 20~50 image sets. Pixel standard deviations of lifetime and anisotropy measurements were influenced by fluorescence brightness, *i.e.* the expression level and the brightness/quenching of the fluorophore.

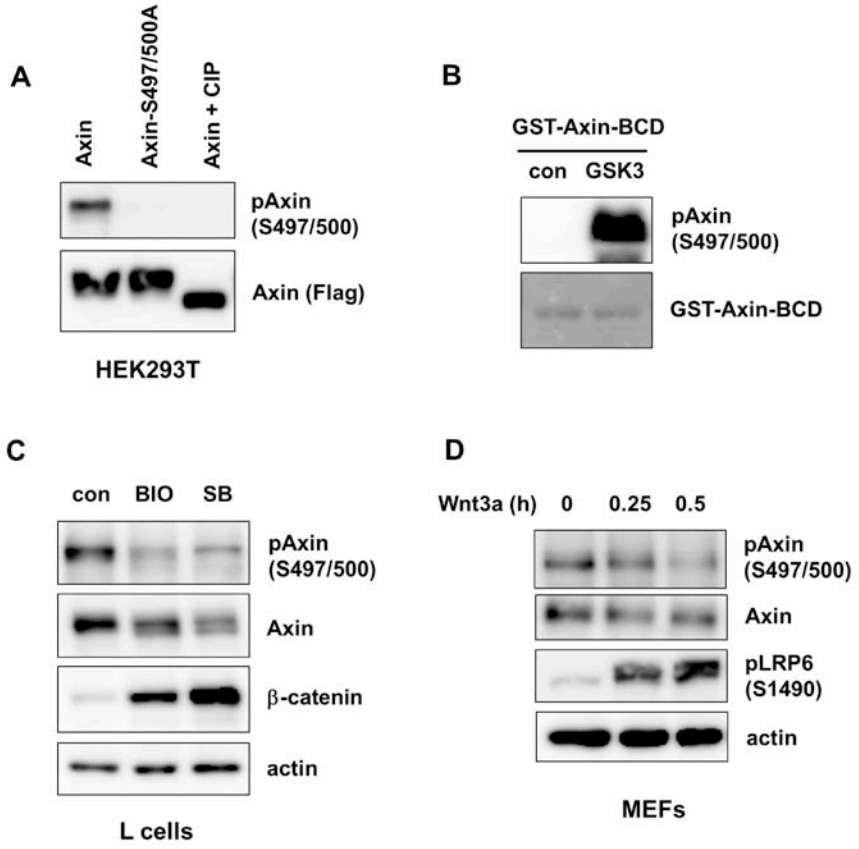

Fig. S1. Characterization of Ab-pS497/500, an antibody for phospho-Axin.

(**A**) Specificity of Ab-pS497/500. HEK293T cells were transfected with an expression vector for Flag-tagged Axin or Axin(S497/500A), which contains alanine substitutions of S497 and S500. Lysates from cells overexpressing Flag-tagged Axin were untreated (lane 1) or treated with calf intestinal phosphatase (CIP) for 1 hour (lane 3), and lysates from cells overexpressing Flag-tagged Axin(S497/S500) were examined by immunoblotting with Ab-pS497/500 (top), or an Flag antibody (bottom). Note that Axin(S497/500A) appeared to be similarly phosphorylated as the WT Axin, as judged by electrophoretic mobility when compared to the WT Axin untreated or treated with CIP (bottom), implying the existence of other phosphorylation sites in addition to S497 and S500.

(**B**) Phosphorylation of Axin at S497 and S500 by GSK3 in vitro. Purified GST-Axin-BCD (β-catenin binding domain), which contains S497 and S500, was phosphorylated by GSK3 in vitro. Axin-BCD phosphorylation was detected by immunoblotting with Ab-pS497/500 (top). GST-Axin-BCD was visualized via Ponceau staining (bottom).

(**C**) Effects of pharmacological inhibitors of GSK3 on phosphorylation at S497 and S500 of the endogenous Axin in L cells. Cells were treated with DMSO (con: control), BIO, or

SB216763 (SB) for 2 hours, and lysates were examined by immunoblotting with indicated antibodies. BIO or SB216753 stabilized β-catenin.

(**D**) Wnt3a-induced dephosphorylation at S497 and S500 of the endogenous Axin in mouse embryonic fibroblasts (MEFs). MEFs were treated with Wnt3a for 0, 0.25 or 0.5 hours. Lysates were examined by immunoblotting with indicated antibodies.

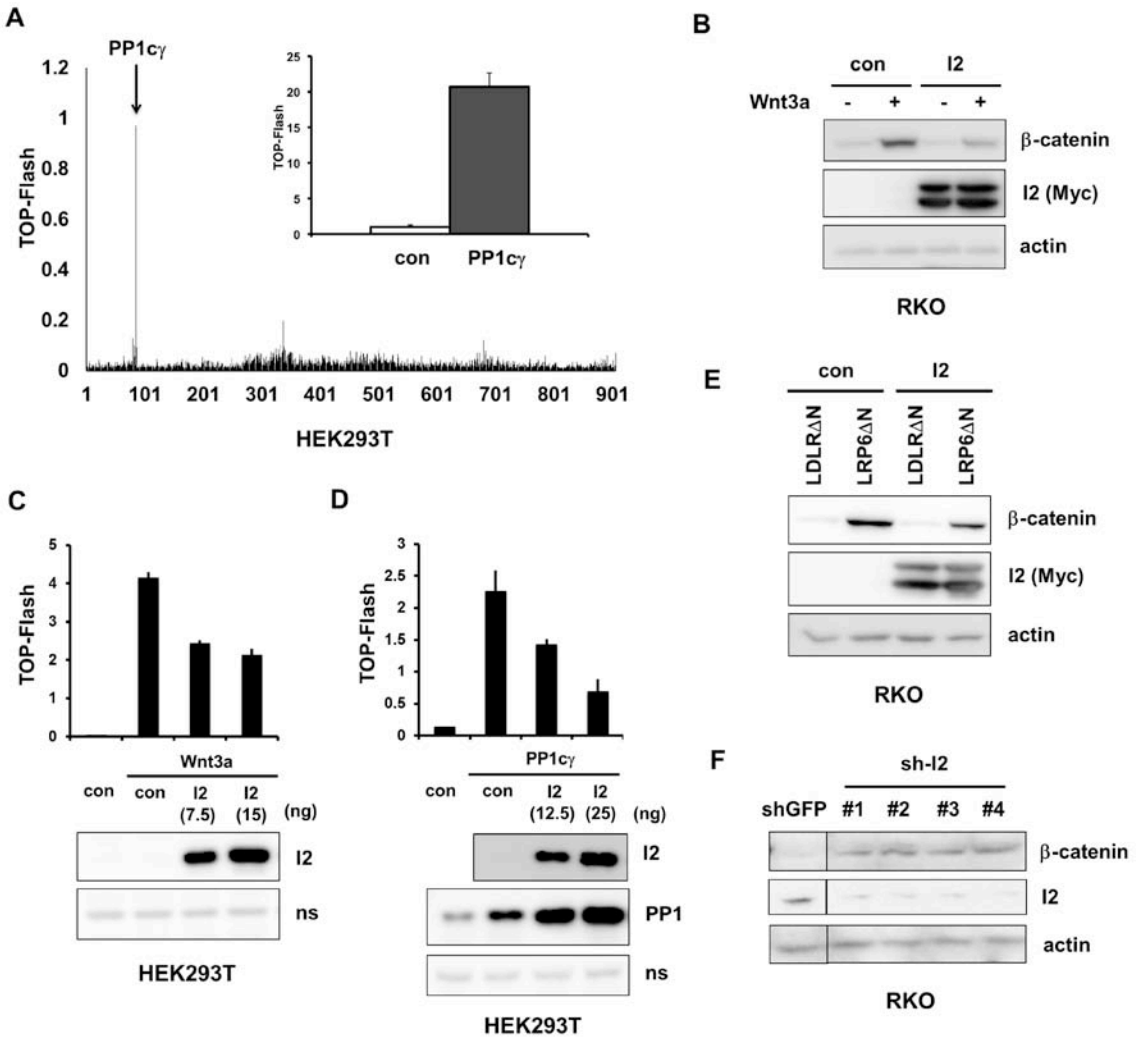

Fig. S2. PP1c activates whereas I2 inhibits Wnt signaling in human cell lines.

(**A**) Identification of PP1cγ as an activator of Wnt signaling. HEK293T cells were transfected with arrayed cDNAs and TOP-Flash reporter activities were monitored. PP1cγ was the most potent activator among 901 cDNAs in this cDNA set. Inset: Confirmation that PP1cγ activated TOP-Flash expression compared to control. Error bars indicate SD of triplicates.

(**B**) Overexpression of I2 inhibited β-catenin stabilization by Wnt3a conditioned medium (CM). Human colon carcinoma RKO cells were transfected with a control or Myc-tagged I2 expression vector (0.25 μg) for 24 hours and were then treated with control L cell CM or Wnt3a CM for an additional 2 hours. Lysates were examined by immunoblotting with indicated antibodies.

(**C** and **D**) Overexpression of I2 inhibited TOP-Flash reporter expression activated by overexpression of Wnt3a (C) or PP1cγ (D). HEK293T cells were co-transfected for 24

hours with expression vectors for Wnt3a (0.5 ng) or PP1cγ (10 ng) and TOP-Flash plus increasing doses of an I2 (or control) expression vector. Error bars indicate SD of triplicates. Lysates were examined by immunoblotting with indicated antibodies (lower panels). ns: a non-specific band for loading control. I2 protein co-expression enhanced the expression level of PP1cγ protein (D).

(**E**) Overexpression of I2 inhibited β-catenin stabilization by overexpression of LRP6ΔN, a constitutively activated LRP6 (*5*). RKO cells were co-transfected with expression vectors for LDLRΔN (control) or LRP6ΔN (0.25 μg) plus Myc-tagged I2 (0.25 μg) for 24 hours. Lysates were examined by immunoblotting with indicated antibodies.

(**F**) Depletion of the endogenous I2 with shRNAs (sh-I2#1 to #4) resulted in stabilization of β-catenin in RKO cells. shGFP: an shRNA against GFP. Lysates were examined by immunoblotting with indicated antibodies.

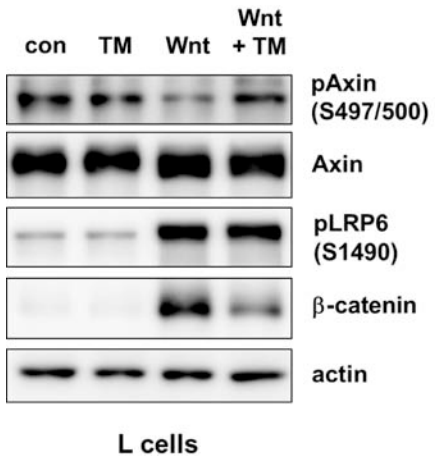

Fig. S3. Tautomycin (TM) inhibits Wnt3a-induced dephosphorylation of Axin in L cells.

L cells were treated with Wnt3a plus TM (2 μM) (or DMSO) for 2 hours. TM inhibited Wnt3a-induced dephosphorylation of Axin and β-catenin stabilization, but did not affect Wnt3a-induced phosphorylation of LRP6.

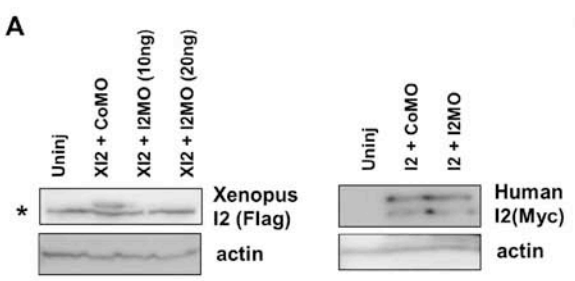

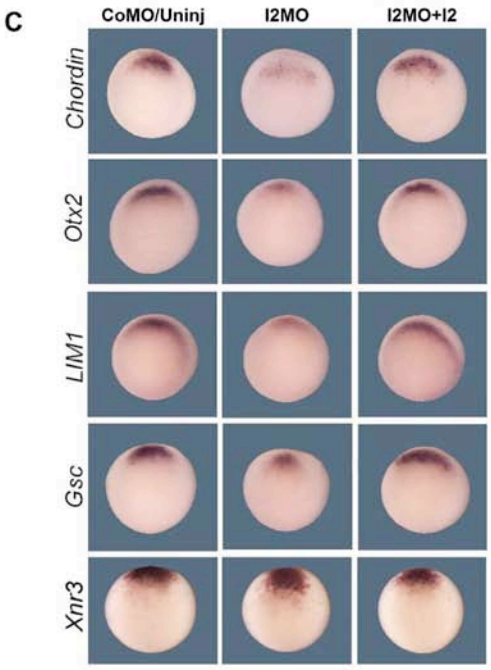

B

	Embryos displaying (%)			
	Normal	Anterior deficiency	DAI	n
Uninj	100	0	5	55
CoMO	100	0	5	36
I2MO	24.3	75.6	3.6 ± 0.1	41
I2MO+I2	82.9	17.1	4.6 ± 0.1	35

D

Percentage of embryos displaying the described changes in marker gene expression

		Uninjected				CoMO				I2MO				I2MO+ I2		
Gene	n	Absent	Reduced	NC	n	Absent	Reduced	NC	n	Absent	Reduced	NC	n	Absent	Reduced	NC
Chordin	27	0	0	100	37	0	5.4	94.6	27	22.2	66.7	11.1	24	0	4.2	95.8
Goosecoid	13	0	0	100	25	0	0	100	21	9.5	85.7	4.8	24	0	16.7	83.3
Otx-2	18	0	0	100	29	0	0	100	30	13.3	83.3	3.3	26	0	23.1	76.9
LIM-1	11	0	0	100	13	0	0	100	10	0	90	10	17	0	11.8	88.2
Xnr-3	12	0	0	100	15	0	0	100	18	0	16.7	83.3	10	0	0	100

NC=no change

E

F

	Embryo Displaying (%)			
	Normal	Anterior deficiency	Anterior enlargement	n
CoMO	100	0	0	70
I2MO	39	61	0	49
β-catMO	52	0	48	64
I2MO+β-catMO	81	16	3	32

Fig. S4. I2 is required for anterior patterning in Xenopus embryos.

(**A**) An I2MO blocked protein synthesis from Xenopus, but not human, I2 mRNA. Xenopus laevis embryos were co-injected with an I2MO or a control MO (CoMO) at 10 or 20 ng/embryo plus mRNAs for Xenopus I2 (Flag-tagged, left panels) or human I2 (Myc-tagged, right panels) at 200 pg/embryo at dorsal animal blastomeres at the 8-cell stage. 3-5 embryos were collected and embryo extracts were examined by immunoblotting with indicated antibodies. "*" marks a non-specific band cross-reacted with the Flag antibody used (left).

(**B**) Summary of the I2MO phenotype shown in Fig. 1F. Dorsoanterior index (DAI) of 5 is defined as the WT. DAI of 3 indicates severe anterior deficiency. n: number of embryos scored at stage 32.

(**C** and **D**) Expression of head organizer or anterior markers, Chordin, LIM1, Otx2, Gossecoid (Gsc) and of a dorsal marker, Xnr3, was examined by in situ hybridization of Xenopus embryos at stage 10.5-11 (C). Statistical data are tabulated in the table (D). CoMO/Uninj: embryos injected with the control MO (10 ng) or uninjected; I2MO: embryos injected with 10 ng of the I2MO; I2MO+I2: Co-injection of the I2MO with human I2 (Myc-tagged) mRNA (200 pg/embryo). Note the rescue effect by human I2 mRNA. Note also that Xnr3, which is not required for anterior patterning, was minimally affected by the I2MO, indicating a specific effect of the I2MO on anterior and head organizer markers.

(**E** and **F**) A β-catenin MO (β-catMO) rescued anterior deficiency caused by the I2MO. Embryos were scored at the tailbud stage. (**E**) (Upper left) A CoMO-injected or uninjected embryo. (Upper right) I2MO-injected embryos displayed diminished anterior structures. (Lower left) A β-catMO-injected embryo displayed enlarged anterior structures including a radial cement gland. (Lower right) An embryo injected with the I2MO and the β-catMO exhibited relatively normal anterior structures. (**F**) Tabulated data for all embryos scored. Note that the β-catMO alone caused, as reported (*32*), anterior enlargement that is opposite to anterior deficiency caused by the I2MO, and that this β-catMO phenotype was reciprocally rescued by the I2MO.

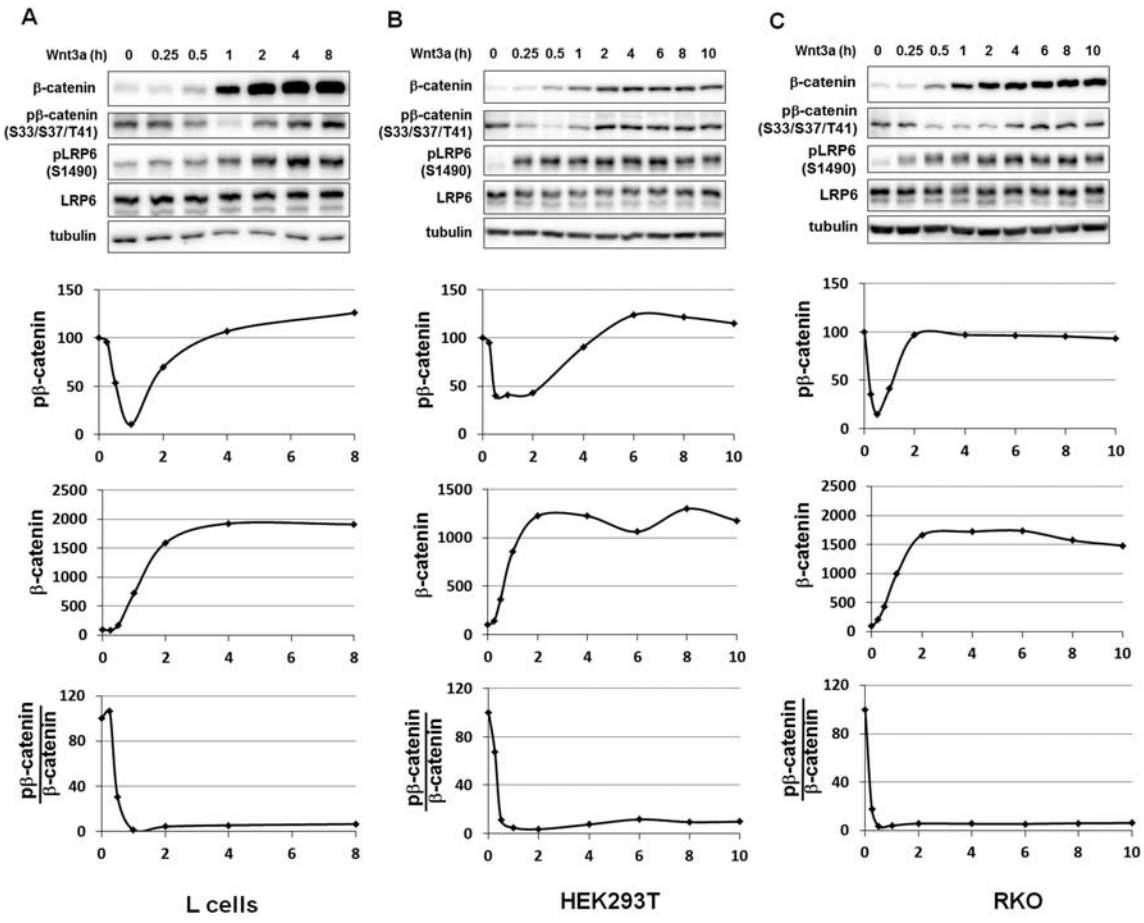

Fig. S5. Kinetics of β-catenin accumulation, β-catenin phosphorylation (at S33/S37/T41) and LRP6 phosphorylation (at S1490) upon Wnt3a treatment.

(**A** to **C**) L (A), HEK293T (B), and RKO (C) cells were treated with Wnt3a (100 ng/ml) for the time indicated. Whole cell lysates were examined by immunoblotting with indicated antibodies except that cytosolic extracts were used for immunoblotting of β-catenin of HEK293T cells (B). β-tubulin was a loading control. Curves represent densitometric quantifications of the level of phospho-β-catenin (top), cytosolic β-catenin (middle), and ratio of phosphorylated β-catenin versus β-catenin (bottom), with x-axes indicating the time of Wnt3a treatment. One representative result was shown for three independent experiments for each cell line. In these three Wnt-responsive cell types, β-catenin phosphorylation decreased within 15 minutes to 2 hours of Wnt3a treatment then recovered. This time course approximately coincided with stabilization of β-catenin reaching a plateau, which represents a new steady state (*24*) where β-catenin synthesis and degradation achieve equilibrium (i.e., the absolute level of β-catenin phosphorylation and degradation returns to that of the unstimulated condition and thus the amount of β-catenin remains unchanged at the plateau level). When normalized to concentrations of β-catenin, however, the relative amount of β-catenin phosphorylation, which reflects the rate of each β-catenin being phosphorylated, was kept low for the entire 8 or 10 hours of

Wnt3a treatment. Note that Wnt3a-induced LRP6 phosphorylation was sustained for the same prolonged periods of 8 to 10 hours as well, mirroring suppression of the rate of β-catenin phosphorylation.

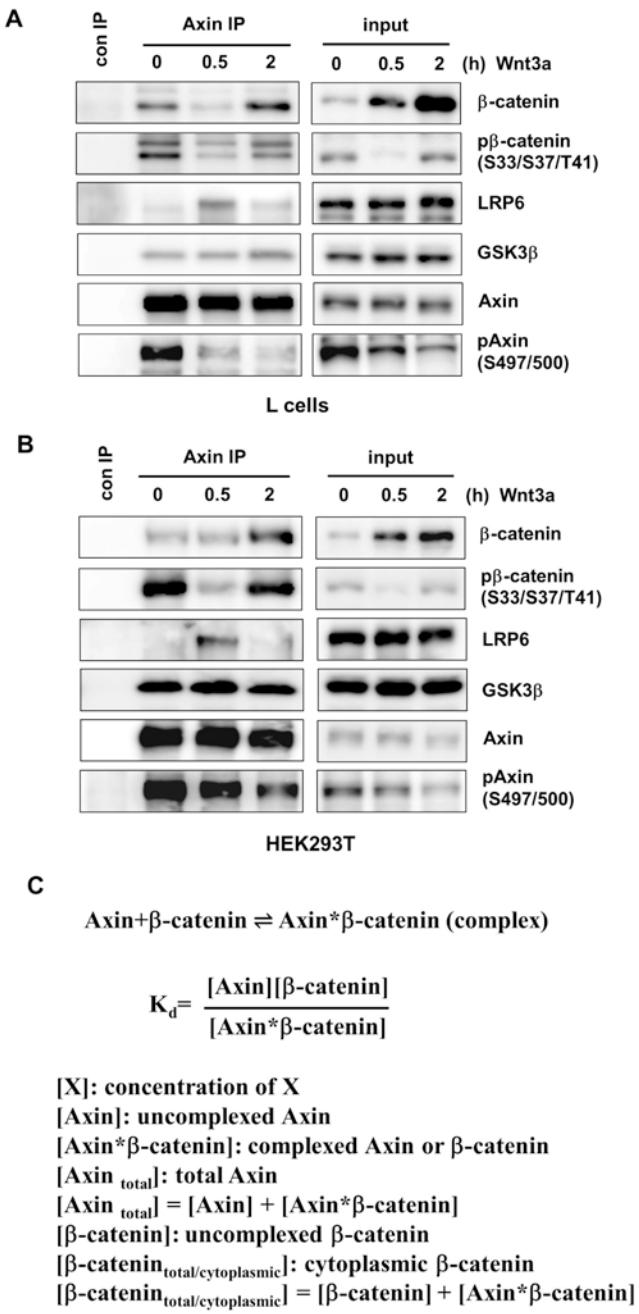

Fig. S6. Wnt3a regulation of Axin-β-catenin and Axin-LRP6 association.

(**A** and **B**) Immunoprecipitation (IP) of Axin and Axin-associated β-catenin, phospho-β-catenin (S33/S37/T41), LRP6, and GSK3 at 0, 0.5 and 2 hours of Wnt3a treatment in L cells (A) and HEK293T cells (B). Each protein examined was endogenous. Con IP: IP with a control IgG. Input lanes were from whole cell lysates except for β-catenin of HEK293T cells (B), which was detected using cytosolic extracts. Quantifications of these experiments in triplicates were shown in Fig. 2. Note that association of Axin and GSK3 appeared to be unchanged with or without Wnt3a stimulation.

Two bands of phospho-β-catenin were detected in Axin IP samples but not input samples of L cells (A). The size of the lower band corresponds to that of β-catenin. The size of the upper band (about 8 kD bigger) led us to speculate that it may correspond to mono-ubiquitinated β-catenin, which normally should exist as a transient (and undetectable) intermediate product en route to be poly-ubiquitinated but somehow became detectable in the Axin destruction complex in L cells. But we have not experimentally verified this speculation.

We note that Axin protein levels were not or minimally affected by Axin dephosphorylation or Wnt3a stimulation in L cells (A and Fig. 1A), or in HEK293T cells within the 2-hour Wnt3a treatment window of our study (B). Axin protein degradation has been observed upon prolonged (4 or more hours) Wnt stimulation in some cells, but this time course lags behind that of stabilization of β-catenin (*16*, *17*). Therefore a decrease of Axin protein levels is unlikely a universal or primary response of Wnt signaling. See more discussion on the subject (*1*).

(**C**) Equations and definitions used for the dissociation constant (Kd) for Axin-β-catenin binary association before and after Wnt3a treatment. A higher Kd indicates a weaker interaction. Data (experiments in A and B in triplicates) at 0-hour (without Wnt3a) and 0.5-hour (with Wnt3a) were used for estimation of Kd changes at these two time points. Note that phosphorylation (at the amino terminus) of β-catenin has no effect on its Axin-binding (*34*), which is mediated by the central domain of β-catenin. In HEK293T cells (B), [Axin*β-catenin] was the same at 0-hour and 0.5-hour, and thus [Axin] must have remained the same because [$Axin_{total}$] did not change, and [β-catenin] must have increased because [$\beta\text{-catenin}_{total/cytoplasmic}$] increased. Therefore the Kd at 0.5-hour, $Kd_{0.5}$, must be higher than Kd_0, the Kd at 0-hour. In L cells (A), [Axin*β-catenin] at 0.5-hour was reduced compared to that at 0 hour, and thus [Axin] must have increased because [$Axin_{total}$] did not change, and [β-catenin] must have increased because [$\beta\text{-catenin}_{total/cytoplasmic}$] increased. Therefore $Kd_{0.5}$ must have increased compared to Kd_0. We note that at 0.5-hour of Wnt3a treatment, [β-catenin] was not at the level that saturated available Axin in either cell type, because [Axin*β-catenin] could be increased by TM or I2 expression, i.e., uncomplexed Axin molecules were present and could be made available for association with β-catenin by TM or I2 (Fig. 3B and 3C). At longer hours of Wnt3a treatment, Axin-β-catenin interaction appeared to be weakened further as suggested by the in vitro binding assay (Fig. 3A).

We note that some of our primary data on Axin immunoprecipitation (Fig. S6B) and β-catenin phosphorylation (Fig. S5) in HEK293T cells are similar to those by Li et al (*22*). However our interpretation that Wnt signaling weakens Axin-β-catenin interaction and inhibits β-catenin phosphorylation contrasts that by these authors. Li et al. propose that Wnt signaling inhibits neither Axin-β-catenin interaction nor β-catenin phosphorylation but inhibits β-catenin ubiquitination; in doing so Wnt signaling maintains an intact Axin destruction complex in which phospho-β-catenin stably binds to and saturates Axin,

thereby keeping newly synthesized (and unphosphorylated) β-catenin from association with Axin and leading to β-catenin accumulation (*22*).

Li et al's interpretation appears to derive in part from the observation that the level of β-catenin phosphorylation, cytosolic or in Axin immunoprecipitates, was not reduced under Wnt stimulation (*22*). We (Fig. S5 and S6B) and others (*24*) have observed similar results under Wnt stimulation at 2 or longer hours when Wnt-induced β-catenin accumulation has reached the plateau. This plateau represents a new steady state (*24*) when β-catenin synthesis equals its degradation, i.e., the level of β-catenin phosphorylation (and degradation) recovers to the level prior to Wnt stimulation (Fig. S5). However the rate of β-catenin phosphorylation, defined by the amount of phospho-β-catenin divided by the amount of cytosolic β-catenin, was inhibited throughout Wnt stimulation (Fig. S5) (*3*, *24*). Relatedly, the rate of β-catenin phosphorylation in the Axin complex, defined by the amount of Axin-associated phospho-β-catenin divided by the amount of Axin-associated β-catenin, was inhibited by Wnt stimulation (Fig. 2B, middle panel, and Fig. S6B). These findings are similar to those observed under Wnt stimulation by Li et al when they equalized the level of β-catenin using a proteasome inhibitor (*22*).

Regarding to Axin-β-catenin interaction, Li et al. (*22*) and we both observed higher amounts of β-catenin associated with Axin upon Wnt stimulation (at 2 hours, Fig. S6B), but normalization to the level of β-catenin showed weakened Axin-β-catenin association (Fig. 2B, left panel) as reported (*17*), a conclusion further supported by our more quantitative estimation of Kd changes for Axin-β-catenin interaction before and after Wnt3a treatment. Therefore one key difference resulting in these contrasting interpretations by Li et al and this study is that we normalized the amount of phospho-β-catenin and the amount of β-catenin associated with Axin to that of β-catenin (Fig. 2 and Fig. S5) while Li et al. did not (*22*).

In our view Li et al's model faces some conceptual challenges. Firstly, as newly synthesized (unphosphorylated) β-catenin proteins accumulate to high levels, how could these β-catenin molecules be prevented from competing for binding to Axin, given that phospho-β-catenin and (unphosphorylated) β-catenin bind equally to Axin (*34*)? Secondly, Li et al's model predicts a continuous rise of the β-catenin level under Wnt stimulation without plateauing. This would contradict the observed plateau of Wnt-induced β-catenin accumulation unless another mechanism is assumed to turn off β-catenin synthesis.

Our experimental evidence and interpretation agree fully with the prevailing model that Wnt signaling stabilizes β-catenin through inhibition of β-catenin phosphorylation (*1*, *11*, *14*, *15*). Quantitative measurements and kinetic modeling of β-catenin phosphorylation based on laws of chemistry further supports this model (*24*).

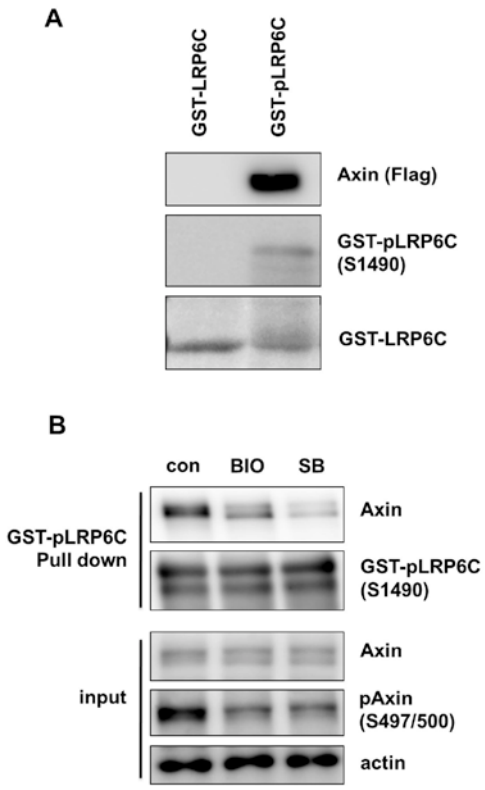

Fig. S7. Association of Axin with GST-phospho-LRP6C in vitro and dependence of this association on Axin phosphorylation by GSK3.

(**A**) Axin associated with GST-phospho-LRP6C specifically. GST-LRP6C was phosphorylated by purified GSK3 and CK1 in vitro and then washed extensively to remove these two kinases, yielding GST-phospho-LRP6C. Axin in cell lysates was incubated with and precipitated by immobilized GST-phospho-LRP6C (or GST-LRP6C), and the associated Axin was detected by immunoblotting. Endogenous Axin (Fig. 3A) from HEK293T cells or Flag-tagged Axin (shown here) from transfected HEK293T cells exhibited specific binding to phospho-LRP6C but not LRP6C (top) as we have described (*6*). Phospho-LRP6C was detected by immunoblotting for S1490 phosphorylation (middle) (*6*). Input GST-LRP6C and GST-phospho-LRP6C were detected by Ponceau staining (bottom), which illustrated a smeary appearance of GST-phospho-LRP6C resulted from phosphorylation as we have reported (*6*).

(**B**) Lysates of HEK293T cells that had been treated for 2 hours with DMSO (con), BIO, or SB216763 (SB) were incubated with and precipitated by immobilized GST-phospho-LRP6C. Associated Axin from the lysates was detected by immunoblotting, and so were input Axin and phospho-Axin (at S497/500), and GST-phospho-LRP6C (at S1490). Reduction of Axin association with GST-phospho-LRP6C caused by BIO or SB appeared to be correlated with reduced phosphorylation of Axin by GSK3.

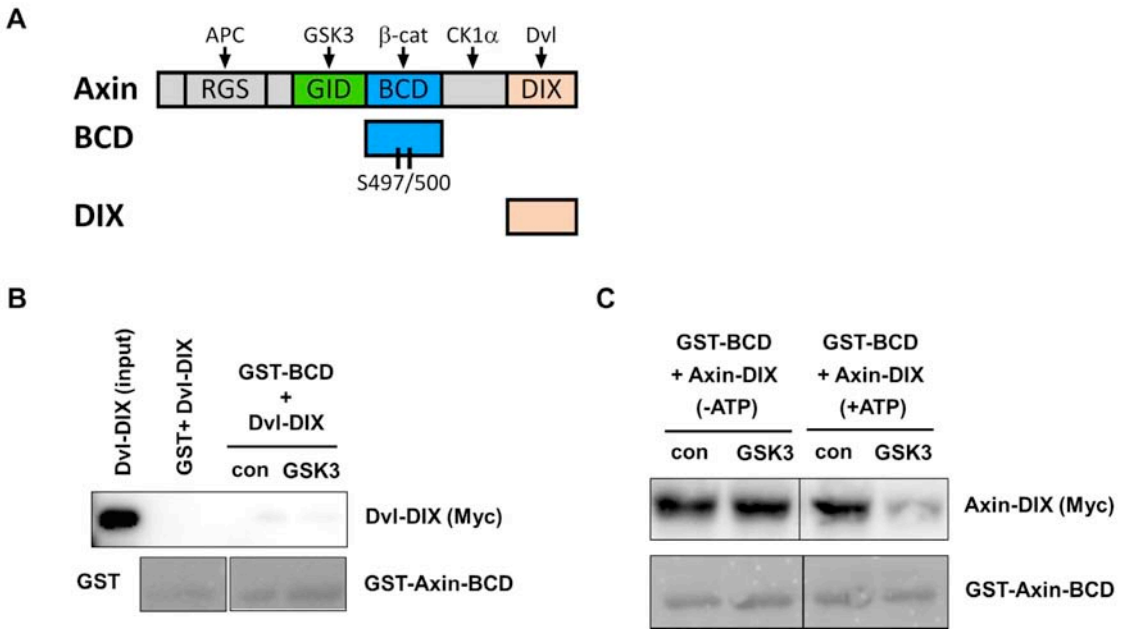

Fig. S8. Specific binding between recombinant Axin-BCD and Axin-DIX fragments in vitro and its inhibition through Axin-BCD phosphorylation by GSK3.

(**A**) Schematic representation of Axin, and Axin-BCD and Axin-DIX fragments. Some key Axin partners are indicated on top. RGS: "regulator of G-protein signaling" domain. GID: GSK3-interacting domain. Note that BCD contains S497 and S500.

(**B**) DVL-DIX, in contrast to Axin-DIX (Fig. 4A), did not associate with GST-Axin-BCD. This experiment was done together with that in Fig. 4A with Dvl-DIX serving as a negative control for Axin-DIX in binding to Axin-BCD, thereby demonstrating the specificity of this in vitro binding assay. Also see fig. S12A to S12C.

(C) Association of Axin-BCD with Axin-DIX was inhibited by GSK3 phosphorylation of Axin-BCD. GST-Axin-BCD was incubated with GSK3 with or without ATP and was then used to precipitate Axin-DIX. Phosphorylation of Axin-BCD by GSK3 (+ATP), but not GSK3 *per se* (-ATP), resulted in reduced BCD-DIX binding.

Binding assays (B and C) were performed as those in Fig. 4A and 4B using recombinant proteins expressed and purified from bacteria and purified GSK3 from a commercial source. Axin-DIX and Dvl-DIX were each Myc-tagged and were detected by immunoblotting, and GST and GST-Axin-BCD were detected by Ponceau staining.

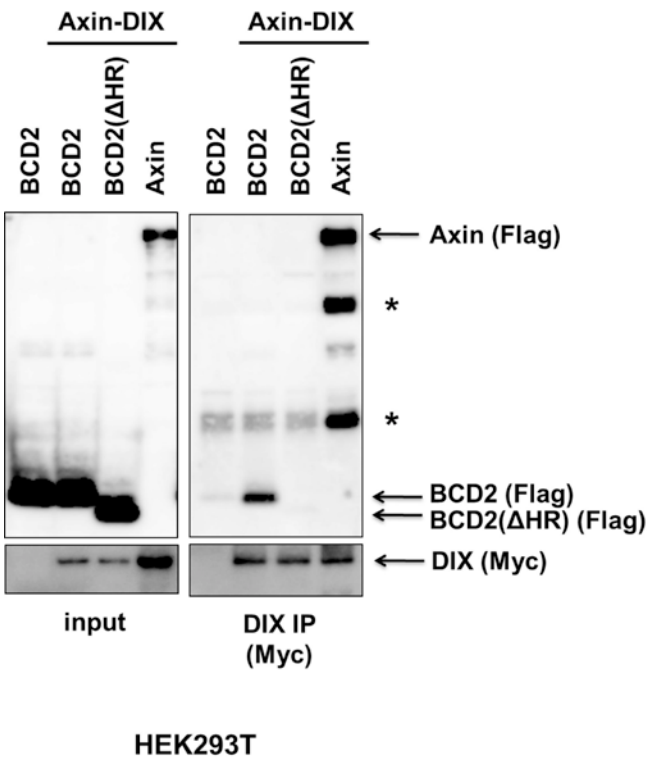

Fig. S9. Association between Axin-BCD and Axin-DIX fragments expressed in HEK293T cells.

Axin-DIX co-immunoprecipitated Axin and Axin-BCD2, but not Axin-BCD2(ΔHR). Axin-BCD2 lacks BCD's N-terminal 46 residues (fig. S11), which appeared to be dispensable for association of BCD with DIX. Axin-BCD2(ΔHR) has a deletion of BCD's histidine-rich (HR) region (fig. S11), which appeared to be essential for association of BCD with DIX (also see fig. S10B). Axin, Axin-BCD2, and Axin-BCD2(ΔHR) were each Flag-tagged while Axin-DIX was Myc-tagged. Bands marked by "*", which were present in Axin-DIX (Myc) immunoprecipitates only, likely represent proteolytic fragments of Axin occurred during immunoprecipitation procedures. Expression vectors for the indicated proteins or fragments were transfected alone to together into HEK293T cells. Cell lysates were subjected to immunoprecipitation with a Myc antibody.

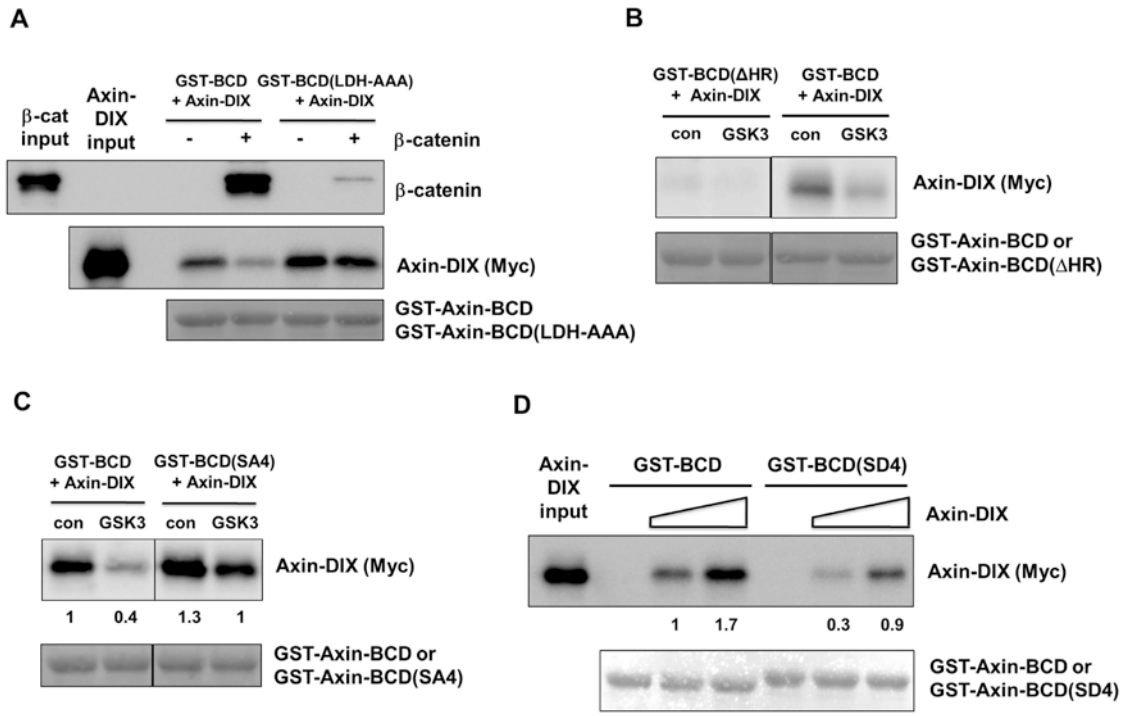

Fig. S10. Mapping residues of Axin-BCD that are involved in BCD-DIX interaction or mediate the inhibitory effect of GSK3 phosphorylation on BCD-DIX interaction.

In vitro binding assays in this figure were performed similarly as those in Fig. 4A and 4B and fig. S8 using recombinant proteins expressed and purified from bacteria and purified GSK3 from a commercial source. Axin-DIX (Myc-tagged) and β-catenin were detected by immunoblotting, and GST-Axin-BCD and GST-Axin-BCD mutants were detected by Ponceau staining.

(**A**) β-catenin and Axin-DIX bind to different regions of Axin-BCD and compete for Axin-BCD through steric hindrance. GST-Axin-BCD(LDH-AAA) contains alanine substitutions of conserved leucine, aspartic acid, and histidine in the β-catenin-binding α-helix (*34*) (fig. S11), and bound minimally to β-catenin (top panel) as reported (*34*). GST-Axin-BCD(LDH-AAA) bound to Axin-DIX similarly as GST-Axin-BCD did, but the binding was not competed by β-catenin (middle panel). By contrast, Axin-DIX association with GST-Axin-BCD was competed by β-catenin (middle panel), demonstrating that β-catenin competition with Axin-DIX for binding to Axin-BCD depends on β-catenin binding to Axin-BCD.

(**B**) Axin-DIX associated with GST-Axin-BCD but not GST-Axin-BCD(ΔHR), which has a deletion of the histidine-rich (HR) region of BCD (fig. S11). This result suggests that the HR region of BCD is required for BCD-DIX interaction, consistent with that observed in HEK293T cells (fig. S9).

(**C**) Axin-DIX exhibited stronger association with GST-Axin-BCD(SA4) than with GST-Axin-BCD, and the association was more resistant to inhibition by GSK3 phosphorylation. GST-Axin-BCD(SA4) contains alanine substitutions of 4 serine/threonine residues including S497 and S500 in BCD (fig. S11). The relative intensity of associated Axin-DIX is indicated. Thus these 4 serine/threonine residues appeared to be responsible for a significant part, but not all, of the inhibitory effect of BCD phosphorylation by GSK3 on BCD-DIX interaction. GSK3 may phosphorylate other residues in addition to these 4 serines/threonines in BCD.

(**D**) Axin-DIX exhibited weaker association with GST-Axin-BCD(SD4) than GST-Axin-BCD. GST-Axin-BCD(SD4) contains phosphomimetic aspartic acid substitutions of 4 serine/threonine residues including S497 and S500 in BCD (fig. S11), and exhibited approximate 50% and 70% reductions in binding to two doses (at 1X and 3X) of Axin-DIX, determined by the relative intensity of associated Axin-DIX. Thus negative charges at these 4 amino acid positions appeared to partially mimic the effect of serine/threonine phosphorylation by GSK3. This is consistent with the possibility that GSK3 may phosphorylate additional residues in addition to these 4 serines/threonines in BCD.

Results in (B), (C), and (D), and fig. S9 together suggest that positive charges of the HR region are required for, whereas negative charges generated in BCD through phosphorylation by GSK3 antagonize, the association of Axin-BCD with Axin-DIX.

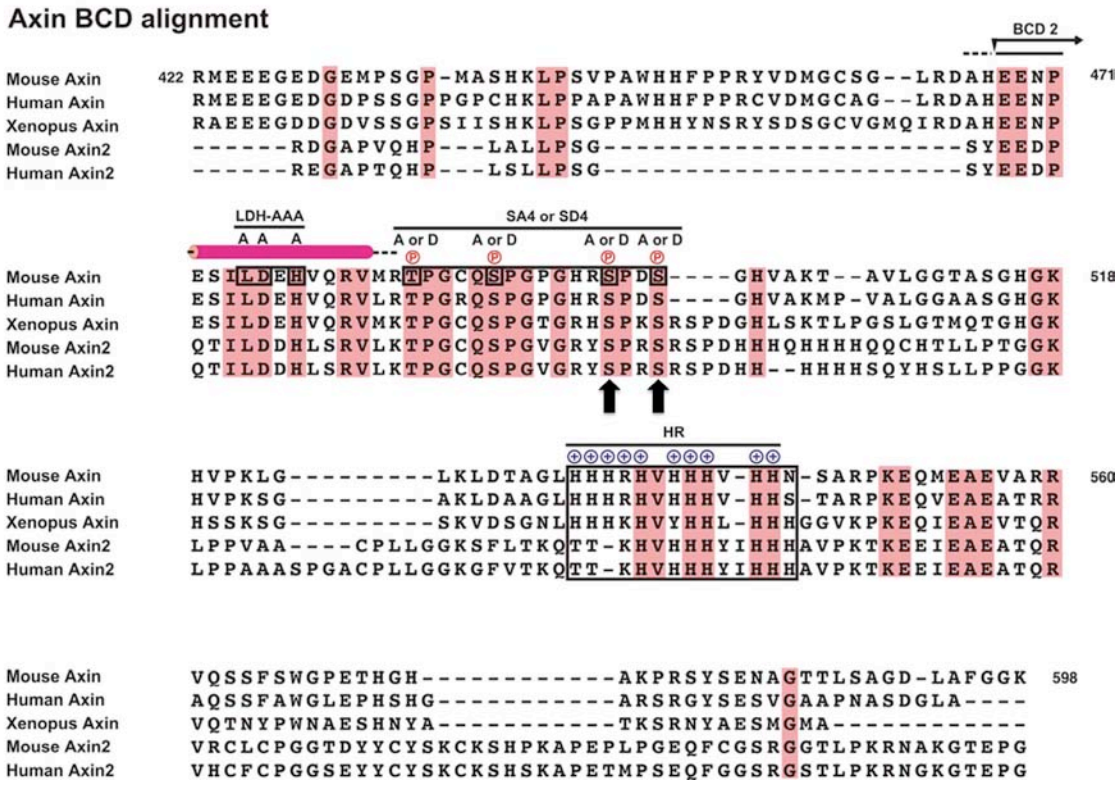

Fig. S11. BCD sequence alignment among Axin proteins.

The BCD of the mouse Axin, which was used in this paper, is listed on top and aligned with the BCD of human and Xenopus Axin, and mouse and human Axin2. Identical residues are shaded in red. The β-catenin-binding α-helix, which is the only visible structure from a β-catenin/Axin-BCD (Xenopus) co-crystal (*34*), is shown above the alignment as a red-colored rod. The conserved histidine-rich (HR) region (labeled by positive charges), four GSK3 phosphorylation sites examined including S497 and S500 (indicated by arrows) are highlighted, as are positions of BCD(LDH-AAA) (*34*), BCD(SA4) and BCD(SD4) mutations. The BCD2 gene product, which was examined in fig. S9, lacks the N-terminal 46 residues of the BCD gene product.

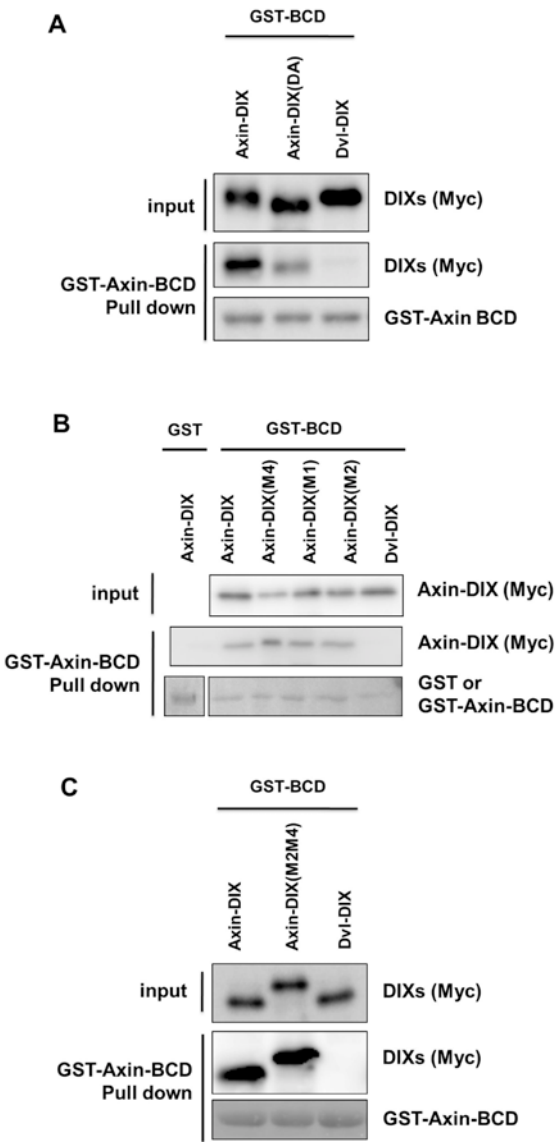

Fig. S12. Mapping residues of Axin-DIX that are involved in the intra-molecular BCD-DIX interaction.

In vitro binding assays in this figure were performed similarly as those in Fig. 4A and 4B, and fig. S8 and S10, using recombinant proteins expressed and purified from bacteria. Axin-DIX, Axin-DIX(DA), and Dvl-DIX were each Myc-tagged and were detected by immunoblotting, and GST and GST-Axin-BCD were detected by Ponceau staining.

(**A**) Axin-DIX(DA), which contains alanine substitutions of 3 aspartic acid and glutamic acid residues in the "DE loop" (between β-strands D and E, fig. S13), exhibited weaker binding to GST-Axin-BCD than Axin-DIX did. Dvl-DIX did not bind to GST-Axin-BCD. This result suggests that the 3 acidic residues in the DE loop are responsible for much, although not all, of the interaction between Axin-DIX and Axin-BCD.

(**B** and **C**) Association of Axin-DIX with Axin-BCD is independent of DIX oligomerization. Axin-DIX is suggested to form homo-oligomers, or hetero-oligomers with Dvl-DIX (*35*, *36*). M1, M2, and M4 mutations (B), and the M2M4 mutation (M2 and M4 combined) (C) of Axin-DIX (fig. S13) are each oligomerization-deficient due to missense mutations in the "head" or "tail" oligomerization interfaces (*35*). These Axin-DIX mutants bound to GST-Axin-BCD similarly as the WT Axin-DIX. Dvl-DIX did not bind to GST-Axin-BCD. Axin-DIX(M2M4) somehow exhibited slower electrophoretic mobility than Axin-DIX (C).

Together with the mapping results on Axin-BCD (fig. S10), it appears that electrostatic attraction between the positively charged HR region of Axin-BCD and the negatively charged DE loop of Axin-DIX contributes to a significant part to BCD-DIX interaction, and that negative charges generated in Axin-BCD through phosphorylation by GSK3 appears to repel the BCD-DIX interaction. Additional interaction interfaces between BCD and DIX may exist.

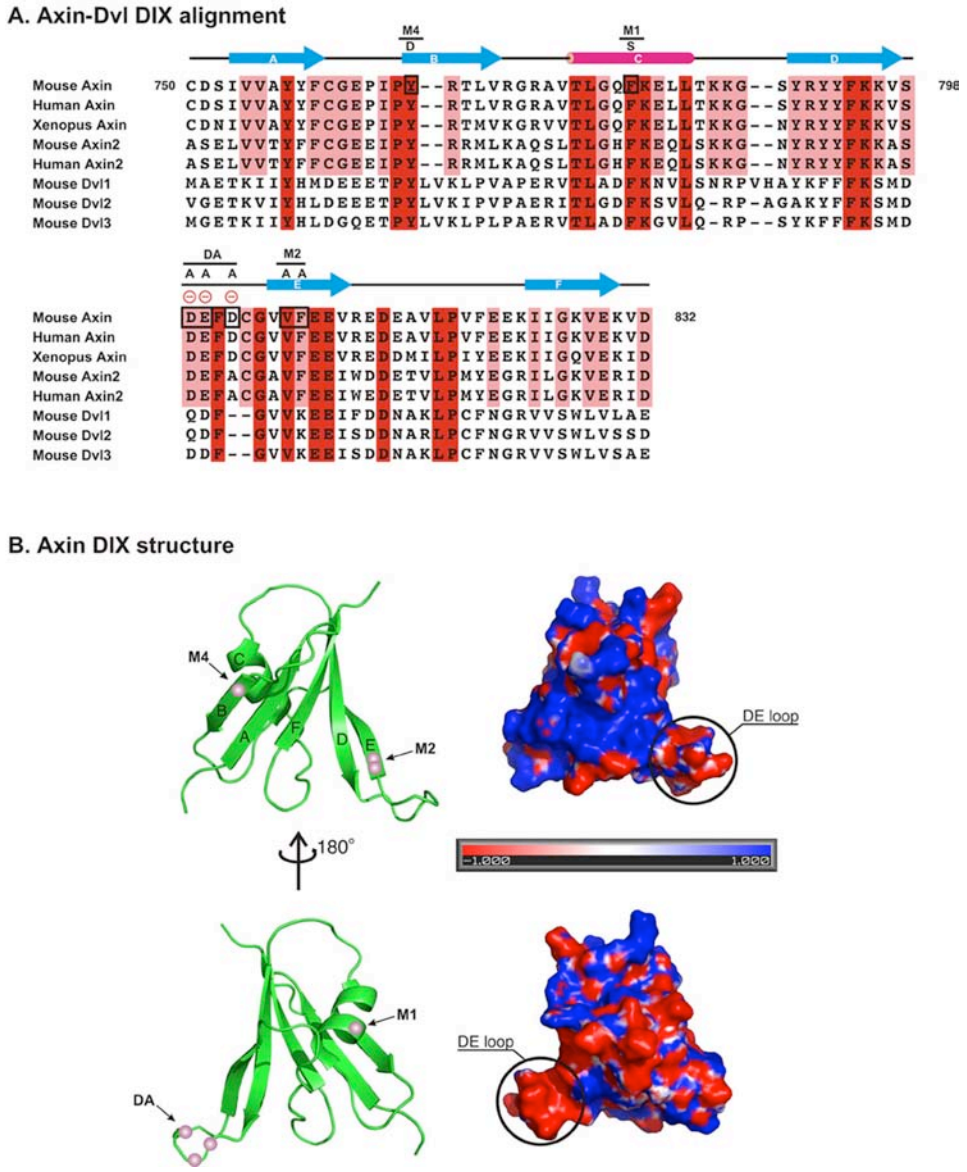

Fig. S13. DIX sequence alignment among Axin and Dvl proteins and an illustration of Axin-DIX structure.

(A) The mouse Axin-DIX, which was used in this paper, is listed on top and aligned with the DIX domain of human and Xenopus Axin, mouse and human Axin2, and mouse Dvl1, Dvl2, and Dvl3. Residues identical among all DIX domains and among Axin DIX domains only are shaded in red and light red, respectively. The secondary structure (β-strands in blue and the α-helix in red) derived from an Axin-DIX crystal structure (*35*) is shown above the alignment. The DE loop, which harbors three D/E residues and is positioned between β-strands D and E, is highlighted by negative charges. Positions and amino acid substitutions of M1, M2, M4 (*35*), and DIX(DA) mutations are shown on top.

(**B**) Axin-DIX structure (PDB accession code 1WSP) (*34*). (Left) Ribbon diagram of an Axin-DIX monomer and its view after 180^{o} rotation. Secondary structural elements are

indicated. (Right) Surface of the Axin-DIX structure and its view after 180^{o} rotation are shown with electrostatic potential (from −1 to 1 kilo teslas). M1, M2, M4 (at the two oligomerization/polymerization interfaces), and DA (in the DE loop) mutations are indicated. The DE loop, which is circled (right panels), is distinct from the oligomerization interfaces and appears to be positioned suitably for interacting with a partner (Axin-BCD).

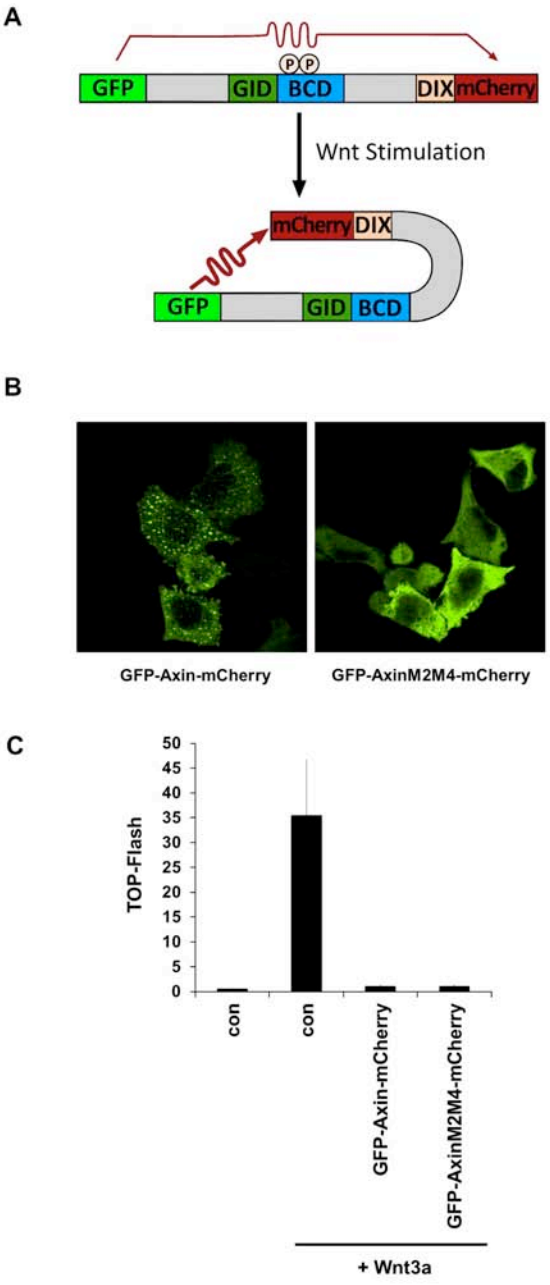

Fig. S14. Design and basic properties of GFP-Axin-mCherry and GFP-AxinM2M4-mCherry for FRET (fluorescence resonance energy transfer)

(**A**) FRET scheme for detection of a Wnt-regulated conformational rearrangement of Axin resulted from the BCD-DIX intra-molecular interaction. We engineered GFP-Axin-mCherry, in which Axin was fused in frame with GFP (green fluorescence protein) and its derivative mCherry at amino and carboxyl termini, respectively (top). We hypothesized that Wnt-induced Axin dephosphorylation promotes the BCD-DIX intra-molecular interaction and results in a closer proximity of amino and carboxyl termini of Axin and thereby stronger FRET from GFP (donor) to mCherry (acceptor) (bottom).

(**B**) A comparison of GFP-Axin-mCherry and GFP-AxinM2M4-mCherry upon overexpression in cells. Likely as a result of DIX oligomerization (*10*, *35*), overexpressed GFP-Axin-mCherry formed cytoplasmic puncta (left), which produced strong inter-Axin GFP-to-mCherry FRET that overwhelmed intra-Axin GFP-to-mCherry FRET that we intended to measure (data not shown). We therefore generated GFP-AxinM2M4-mCherry, which contains the DIX(M2M4) mutation (a combination of M2 and M4 mutations in *cis*, fig. S13) and is unable to oligomerize (*10*, *35*). Note that Axin-DIX(M2M4) was fully capable of association with Axin-BCD (fig. S12C). Overexpressed GFP-AxinM2M4-mCherry showed a diffused pattern in cytosol as anticipated (*10*, *35*) (right). HeLa cells were transfected with an expression vector for GFP-Axin-mCherry (left) or GFP-AxinM2M4-mCherry (right) for 24 hours, and were fixed and examined by confocal microscopy.

(**C**) GFP-AxinM2M4-mCherry appeared to function similarly as GFP-Axin-mCherry when overexpressed, and antagonized Wnt/β-catenin signaling effectively. HEK293T cells were transfected with an expression vector for GFP-Axin-mCherry, GFP-AxinM2M4-mCherry, or a control, plus a Wnt3a expression vector and the TOP-Flash reporter. Error bars represent SD of triplicates.

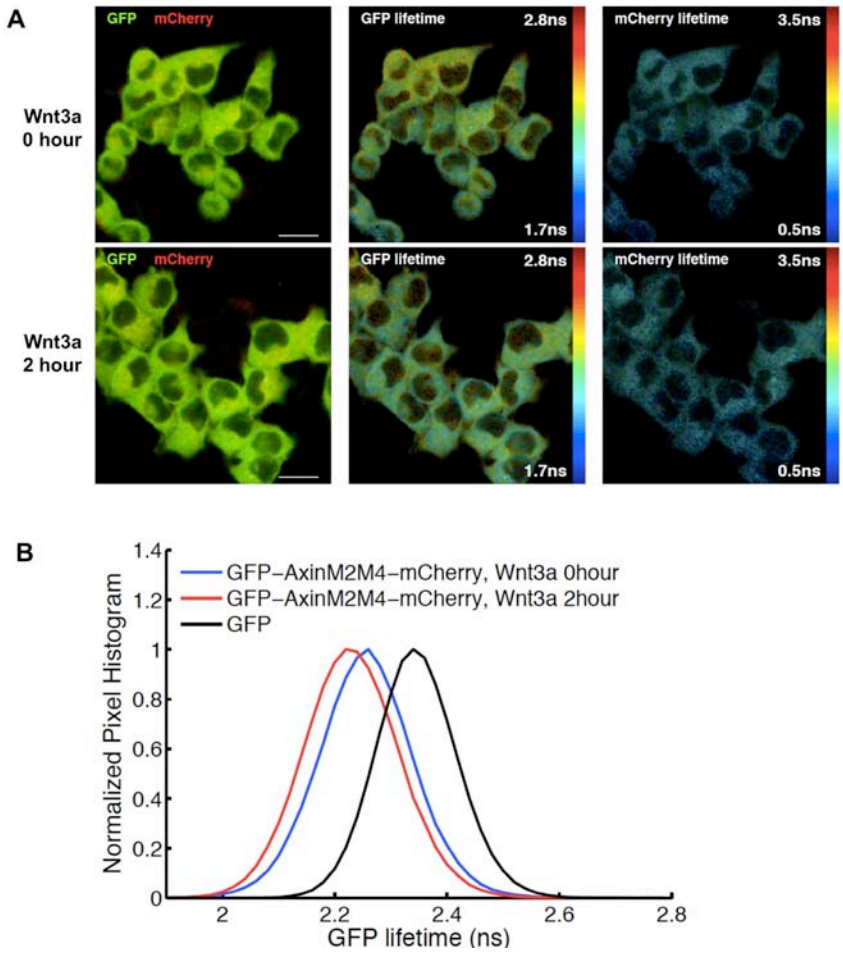

Fig. S15. Wnt enhancement of FRET of GFP-AxinM2M4-mCherry in live cells.

(**A**) FLIM (Fluorescence Lifetime Imaging Microscopy) imaging for FRET measurements in live cells. We used FLIM to measure GFP lifetime shortening, which serves as a more robust FRET indicator. This is because fluorescence lifetime is an intrinsic property of a fluorophore and is not affected by fluctuations of fluorophore intensities (i.e., of expression levels of GFP-AxinM2M4-mCherry) (*37*). Shown are a conventional fluorescence image merged for GFP and mCherry (left), a GFP lifetime image (middle, with a pseudo-color scale from 1.7 to 2.8ns), and a mCherry lifetime image (right, with a pseudo-color scale from 0.5 to 3.5ns) before (0 hour, top) and after Wnt3a treatment (2 hours, bottom). Scale bar: 25 μm. HeLa cells transfected with an expression vector for GFP-AxinM2M4-mCherry were treated with Wnt3a.

(**B**) GFP lifetime shortening of GFP-AxinM2M4-mCherry induced by Wnt3a, an indication of stronger GFP-to-mCherry FRET. The histogram represents an ensemble average of GFP lifetime derived from 20 to 50 live cell image sets (one of which is shown in A). GFP lifetime of GFP-AxinM2M4-mCherry was shorter than that of GFP alone (blue versus black), reflecting GFP-to-mCherry FRET as a result when GFP and mCherry were linked into a single protein by fusion with AxinM2M4 (fig. S14A). GFP lifetime of GFP-AxinM2M4-mCherry was further decreased upon Wnt3a treatment (red

versus blue), indicating stronger FRET and thus a shorter distance between the amino and carboxyl terminal DIX of Axin upon Wnt3a treatment (fig. S14A). Control experiments confirmed that intra-molecular GFP-to-mCherry FRET was fully responsible for Wnt3a-induced GFP lifetime shortening in GFP-AxinM2M4-mCherry (fig. S16).

We note following considerations pertaining to the above GFP lifetime data: (i) GFP lifetime shortening induced by Wnt3a was smaller than that resulted from linking GFP with mCherry into a single polypeptide chain of GFP-AxinM2M4-mCherry. But covalent joining of GFP with mCherry should be considered to be an "extreme" conformational rearrangement of GFP; (ii) the histogram shown is an ensemble average of GFP lifetime because each pixel in image data represented hundreds or more of GFP-AxinM2M4-mCherry molecules. It is conceivable that only a fraction of overexpressed GFP-AxinM2M4-mCherry was affected by Wnt3a, and thus the GFP lifetime shortening based on the entire population may be an underestimate; and (iii) GFP and mCherry are large fluorescence labels. GFP lifetime shortening resulted from GFP-to-mCherry FRET could be used as a qualitative indication of a conformational rearrangement, but may not be suitable for being converted into a quantitative measurement of changes of a distance or conformation.

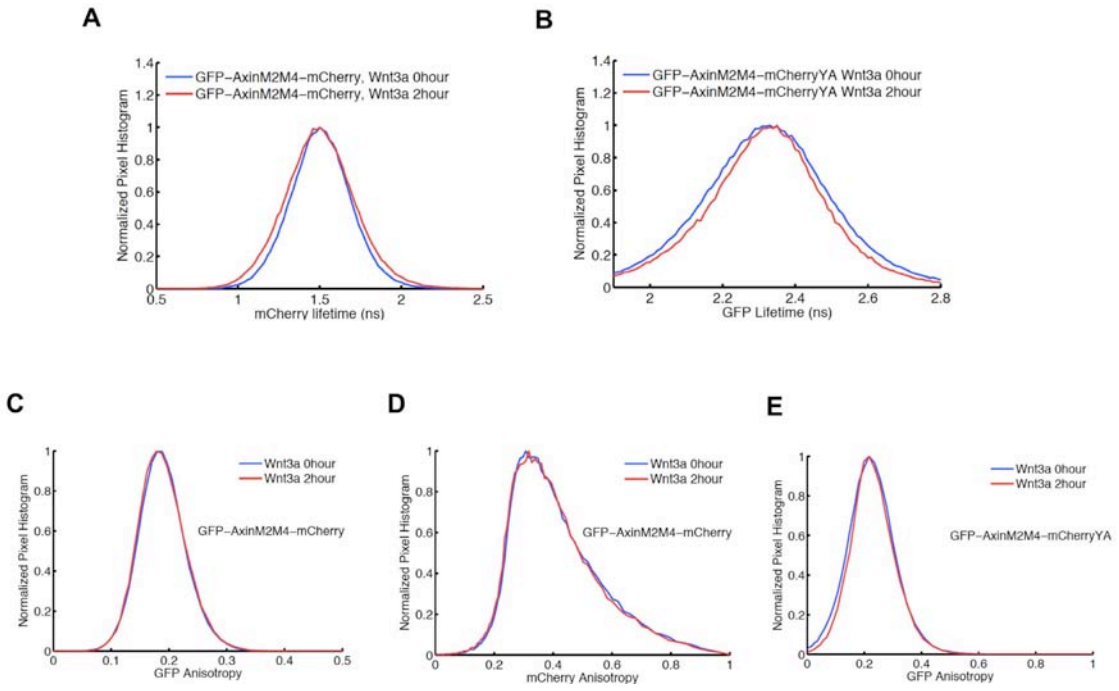

Fig. S16. Control experiments for live cell FLIM imaging and measurements

(**A**) Lifetime of mCherry (FRET acceptor) in GFP-AxinM2M4-mCherry remained unchanged with or without Wnt3a, independent of GFP-to-mCherry FRET. mCherry lifetime also served as an internal control for the imaging system, demonstrating that there was no or negligible baseline drifting in measurement during the live cell experiment that showed a decrease in GFP lifetime (fig. S15B).

(**B**) GFP Lifetime in GFP-AxinM2M4-mCherryYA remained unchanged with or without Wnt3a. The mCherry YA mutation (*38*) is an alanine (A) substitution of the tyrosine (Y) of the MYG tri-peptide that forms the chromophore core (*38*), and thereby renders the mutant mCherry unable to emit or absorb light (while folded properly). GFP-AxinM2M4-mCherryYA did not exhibit any GFP-to-mCherry FRET, because its GFP lifetime remained the same as that of GFP alone (fig. S15B), with or without Wnt3a. This experiment confirmed that the GFP lifetime shortening of GFP-AxinM2M4-mCherry upon Wnt3a treatment (fig. S15B) was a result of GFP-to-mCherry FRET as predicted.

(**C** to **E**) Wnt3a treatment did not cause changes in GFP-AxinM2M4-mCherry inter-molecular interaction, which therefore could not have contributed to the GFP lifetime decrease (fig. S15B). Although AxinM2M4 does not form DIX-mediated oligomers (*35*) (fig. S14B), live cell fluorescence anisotropy imaging (*39*) was performed to rule out experimentally any potential Wnt3a-induced changes in AxinM2M4 dimerization or oligomerization, DIX-mediated or not. Fluorescence anisotropy imaging detects protein oligomerization in cells through homo-FRET measurement between equally labeled proteins (*39*). An elevated oligomerization level would increase inter-Axin GFP-to-GFP FRET and mCherry-to-mCherry FRET, and thus decrease the steady state anisotropy of GFP and mCherry through homo-FRET induced anisotropy decay. Wnt3a did not cause

any changes in steady-state anisotropy and anisotropy decay of either GFP or mCherry in GFP-AxinM2M4-mCherry (C and D). Thus, Wnt3a did not alter GFP-AxinM2M4-mCherry inter-molecular interaction. The same conclusion was also made based on GFP anisotropy measurement using GFP-AxinM2M4-mCherryYA with or without Wnt3a (E).

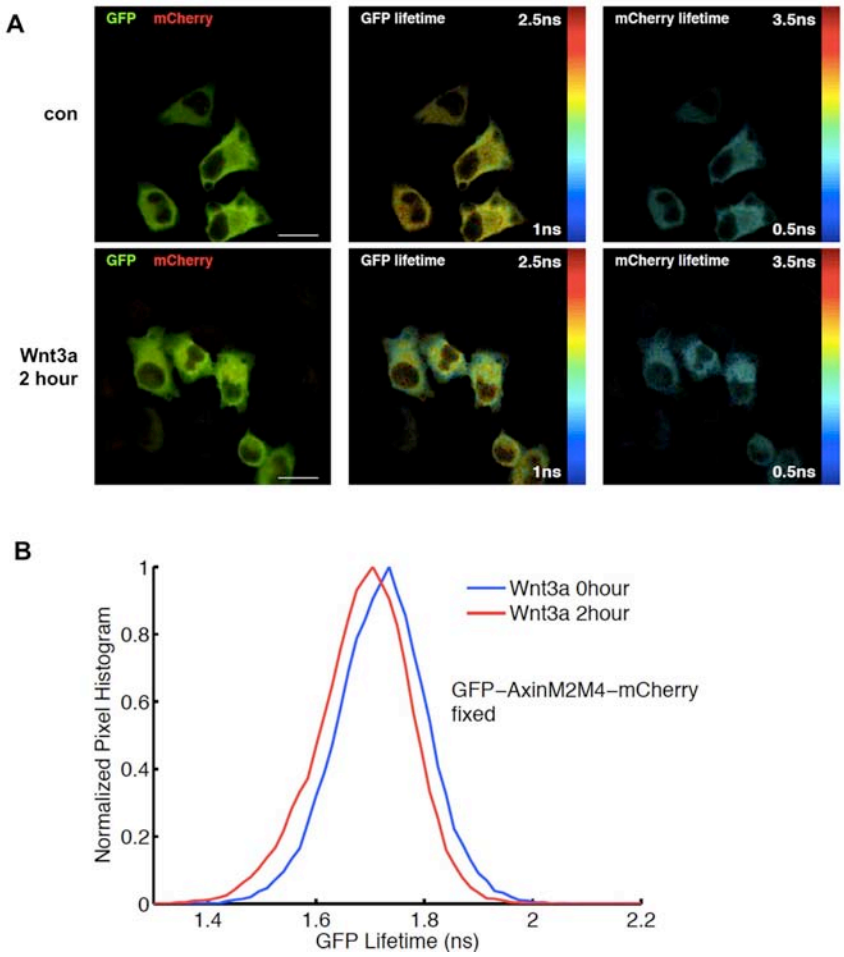

Fig. S17. Wnt-induced GFP lifetime decrease in fixed cells expressing GFP-AxinM2M4-mCherry.

(**A**) HeLa cells transfected with an expression vector for GFP-AxinM2M4-mCherry were untreated or treated with Wnt3a for 2 hours and then fixed. A representative image set is shown for a conventional fluorescence image merged for GFP and mCherry (left), a GFP lifetime image (middle, with a pseudo-color scale from 1 to 2.5ns), and a mCherry lifetime image (right, with a pseudo-color scale from 0.5 to 3.5ns) before (0 hour, top) and after Wnt3a treatment (2 hours, bottom). Scale bar 25 μm.

(**B**) GFP lifetime shortening of GFP-AxinM2M4-mCherry induced by Wnt3a, an indication of stronger GFP-to-mCherry FRET. This result is thus consistent with that of live cell imaging (fig. S15B). GFP lifetime in fixed samples was shorter than that measured in live cell imaging (fig. S15B) as a result of fixation-quenching as commonly observed.

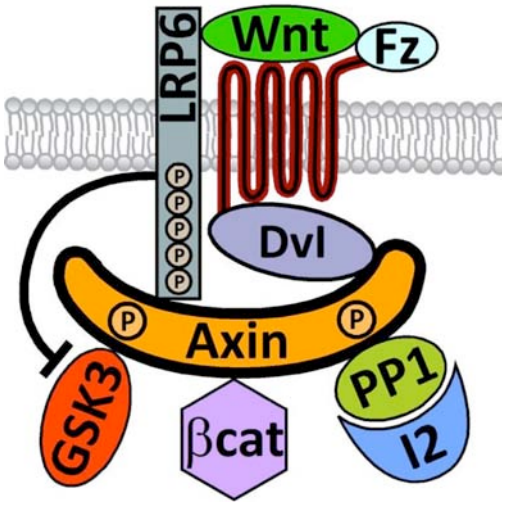

Fig. S18. Comparisons and relations between "direct inhibition of GSK3" versus "Axin inactivation".

Previous studies in vitro by others and us have suggested a model that direct inhibition of GSK3 (in the Axin complex) by phospho-LRP6 upon formation of the LRP6 signaling complex is involved in stabilization of β-catenin (*27-29*). We have likely observed such "direct inhibition of GSK3", because the rate of phosphorylation of β-catenin was reduced in the Axin complex upon Wnt stimulation (Fig. 2A and 2B, middle panel). We cannot make a distinction experimentally on the fraction of β-catenin stabilized through direct inhibition of GSK3 by LRP6 versus that through Axin inactivation by LRP6 (Fig. 4D) because direct inhibition of GSK3 in the Axin complex should favor dephosphorylation and inactivation of Axin by PP1. Thus Axin inactivation by LRP6 could be viewed as a consequence and an 'amplification' step of direct inhibition of GSK3 by LRP6, making it difficult or impossible to separate the effects of these two events in stabilization of β-catenin.

References

1. B. T. MacDonald, K. Tamai, X. He, Wnt/beta-catenin signaling: Components, mechanisms, and diseases. *Dev. Cell* **17**, 9 (2009). doi:10.1016/j.devcel.2009.06.016 Medline

2. H. Clevers, R. Nusse, Wnt/β-catenin signaling and disease. *Cell* **149**, 1192 (2012). doi:10.1016/j.cell.2012.05.012 Medline

3. C. Liu *et al*., Control of beta-catenin phosphorylation/degradation by a dual-kinase mechanism. *Cell* **108**, 837 (2002). doi:10.1016/S0092-8674(02)00685-2 Medline

4. J. Mao *et al*., Low-density lipoprotein receptor-related protein-5 binds to Axin and regulates the canonical Wnt signaling pathway. *Mol. Cell* **7**, 801 (2001). doi:10.1016/S1097-2765(01)00224-6 Medline

5. K. Tamai *et al*., A mechanism for Wnt coreceptor activation. *Mol. Cell* **13**, 149 (2004). doi:10.1016/S1097-2765(03)00484-2 Medline

6. X. Zeng *et al*., A dual-kinase mechanism for Wnt co-receptor phosphorylation and activation. *Nature* **438**, 873 (2005). doi:10.1038/nature04185 Medline

7. G. Davidson *et al*., Casein kinase 1 gamma couples Wnt receptor activation to cytoplasmic signal transduction. *Nature* **438**, 867 (2005). doi:10.1038/nature04170 Medline

8. J. Bilic *et al*., Wnt induces LRP6 signalosomes and promotes dishevelled-dependent LRP6 phosphorylation. *Science* **316**, 1619 (2007). doi:10.1126/science.1137065 Medline

9. X. Zeng *et al*., Initiation of Wnt signaling: Control of Wnt coreceptor Lrp6 phosphorylation/activation via frizzled, dishevelled and axin functions. *Development* **135**, 367 (2008). doi:10.1242/dev.013540 Medline

10. T. Schwarz-Romond, C. Metcalfe, M. Bienz, Dynamic recruitment of axin by Dishevelled protein assemblies. *J. Cell Sci.* **120**, 2402 (2007). doi:10.1242/jcs.002956 Medline

11. C. Metcalfe, M. Bienz, Inhibition of GSK3 by Wnt signalling: Two contrasting models. *J. Cell Sci.* **124**, 3537 (2011). doi:10.1242/jcs.091991 Medline

12. S. Ikeda *et al*., Axin, a negative regulator of the Wnt signaling pathway, forms a complex with GSK-3beta and beta-catenin and promotes GSK-3beta-dependent phosphorylation of beta-catenin. *EMBO J.* **17**, 1371 (1998). doi:10.1093/emboj/17.5.1371 Medline

13. J. Behrens *et al*., Functional interaction of an axin homolog, conductin, with beta-catenin, APC, and GSK3beta. *Science* **280**, 596 (1998). doi:10.1126/science.280.5363.596 Medline

14. D. Kimelman, W. Xu, Beta-catenin destruction complex: Insights and questions from a structural perspective. *Oncogene* **25**, 7482 (2006). doi:10.1038/sj.onc.1210055 Medline

15. J. L. Stamos, W. I. Weis, The β-catenin destruction complex. *Cold Spring Harb. Perspect. Biol.* **5**, a007898 (2013). doi:10.1101/cshperspect.a007898 Medline

16. H. Yamamoto *et al*., Phosphorylation of axin, a Wnt signal negative regulator, by glycogen synthase kinase-3beta regulates its stability. *J. Biol. Chem.* **274**, 10681 (1999). doi:10.1074/jbc.274.16.10681 Medline

17. K. Willert, S. Shibamoto, R. Nusse, Wnt-induced dephosphorylation of axin releases beta-catenin from the axin complex. *Genes Dev.* **13**, 1768 (1999). doi:10.1101/gad.13.14.1768 Medline

18. E. Jho, S. Lomvardas, F. Costantini, A GSK3beta phosphorylation site in axin modulates interaction with beta-catenin and Tcf-mediated gene expression. *Biochem. Biophys. Res. Commun.* **266**, 28 (1999). doi:10.1006/bbrc.1999.1760 Medline

19. W. Luo *et al*., Protein phosphatase 1 regulates assembly and function of the beta-catenin degradation complex. *EMBO J.* **26**, 1511 (2007). doi:10.1038/sj.emboj.7601607 Medline

20. D. M. Virshup, S. Shenolikar, From promiscuity to precision: Protein phosphatases get a makeover. *Mol. Cell* **33**, 537 (2009). doi:10.1016/j.molcel.2009.02.015 Medline

21. C. Niehrs, Regionally specific induction by the Spemann-Mangold organizer. *Nat. Rev. Genet.* **5**, 425 (2004). doi:10.1038/nrg1347 Medline

22. V. S. W. Li *et al*., Wnt signaling through inhibition of β-catenin degradation in an intact Axin1 complex. *Cell* **149**, 1245 (2012). doi:10.1016/j.cell.2012.05.002 Medline

23. V. F. Taelman *et al*., Wnt signaling requires sequestration of glycogen synthase kinase 3 inside multivesicular endosomes. *Cell* **143**, 1136 (2010). doi:10.1016/j.cell.2010.11.034 Medline

24. A. R. Hernández, A. M. Klein, M. W. Kirschner, Kinetic responses of β-catenin specify the sites of Wnt control. *Science* **338**, 1337 (2012). doi:10.1126/science.1228734 Medline

25. A. J. Valvezan, F. Zhang, J. A. Diehl, P. S. Klein, Adenomatous polyposis coli (APC) regulates multiple signaling pathways by enhancing glycogen synthase kinase-3 (GSK-3) activity. *J. Biol. Chem.* **287**, 3823 (2012). doi:10.1074/jbc.M111.323337 Medline

26. B. W. Doble, S. Patel, G. A. Wood, L. K. Kockeritz, J. R. Woodgett, Functional redundancy of GSK-3alpha and GSK-3beta in Wnt/beta-catenin signaling shown by using an allelic series of embryonic stem cell lines. *Dev. Cell* **12**, 957 (2007). doi:10.1016/j.devcel.2007.04.001 Medline

27. G. Wu, H. Huang, J. Garcia Abreu, X. He, Inhibition of GSK3 phosphorylation of beta-catenin via phosphorylated PPPSPXS motifs of Wnt coreceptor LRP6. *PLoS ONE* **4**, e4926 (2009). doi:10.1371/journal.pone.0004926 Medline

28. C. S. Cselenyi *et al*., LRP6 transduces a canonical Wnt signal independently of Axin degradation by inhibiting GSK3's phosphorylation of beta-catenin. *Proc. Natl. Acad. Sci. U.S.A.* **105**, 8032 (2008). doi:10.1073/pnas.0803025105 Medline

29. S. Piao *et al*., Direct inhibition of GSK3beta by the phosphorylated cytoplasmic domain of LRP6 in Wnt/beta-catenin signaling. *PLoS ONE* **3**, e4046 (2008). doi:10.1371/journal.pone.0004046 Medline

30. J. G. Zalatan, S. M. Coyle, S. Rajan, S. S. Sidhu, W. A. Lim, Conformational control of the Ste5 scaffold protein insulates against MAP kinase misactivation. *Science* **337**, 1218 (2012). doi:10.1126/science.1220683 Medline

31. K. Tamai *et al*., LDL-receptor-related proteins in Wnt signal transduction. *Nature* **407**, 530 (2000). doi:10.1038/35035117 Medline

32. J. Heasman, M. Kofron, C. Wylie, Beta-catenin signaling activity dissected in the early *Xenopus* embryo: A novel antisense approach. *Dev. Biol.* **222**, 124 (2000). doi:10.1006/dbio.2000.9720 Medline

33. M. Zhao, L. L. Peng, Multiplexed fluorescence lifetime measurements by frequency-sweeping Fourier spectroscopy. *Opt. Lett.* **35**, 2910 (2010). doi:10.1364/OL.35.002910 Medline

34. Y. Xing, W. K. Clements, D. Kimelman, W. Xu, Crystal structure of a beta-catenin/axin complex suggests a mechanism for the beta-catenin destruction complex. *Genes Dev.* **17**, 2753 (2003). doi:10.1101/gad.1142603 Medline

35. T. Schwarz-Romond *et al*., The DIX domain of Dishevelled confers Wnt signaling by dynamic polymerization. *Nat. Struct. Mol. Biol.* **14**, 484 (2007). doi:10.1038/nsmb1247 Medline

36. M. Fiedler, C. Mendoza-Topaz, T. J. Rutherford, J. Mieszczanek, M. Bienz, Dishevelled interacts with the DIX domain polymerization interface of Axin to interfere with its function in down-regulating β-catenin. *Proc. Natl. Acad. Sci. U.S.A.* **108**, 1937 (2011). doi:10.1073/pnas.1017063108 Medline

37. H. Wallrabe, A. Periasamy, Imaging protein molecules using FRET and FLIM microscopy. *Curr. Opin. Biotechnol.* **16**, 19 (2005). doi:10.1016/j.copbio.2004.12.002 Medline

38. B. R. Martin, T. J. Deerinck, M. H. Ellisman, S. S. Taylor, R. Y. Tsien, Isoform-specific PKA dynamics revealed by dye-triggered aggregation and DAKAP1alpha-mediated localization in living cells. *Chem. Biol.* **14**, 1031 (2007). doi:10.1016/j.chembiol.2007.07.017 Medline

39. M. Tramier, M. Coppey-Moisan, Fluorescence anisotropy imaging microscopy for homo-FRET in living cells. *Methods Cell Biol.* **85**, 395 (2008). doi:10.1016/S0091-679X(08)85017-0 Medline